Beyond 1.0 W cm–2 Performance without Platinum: The Beginning of a New Era in Anion Exchange Membrane Fuel Cells

Travis J. Omasta, Xiong Peng, Hamish R Miller, Francesco Vizza, Lianqin Wang, John R. Varcoe, Dario R Dekel, William E. Mustain

JES Focus Issue on Electrocatalysis — In Honor of Radoslav Adzic

Beyond 1.0 W cm^{-2} Performance without Platinum: The Beginning of a New Era in Anion Exchange Membrane Fuel Cells

Travis J. Omasta,[1,2,=,*] Xiong Peng,[1,2,=,*] Hamish A. Miller,[3] Francesco Vizza,[3] Lianqin Wang,[4] John R. Varcoe,[4,] Dario R. Dekel,[5,z] and William E. Mustain[1,2,**,z]**

[1]*Department of Chemical Engineering, University of South Carolina, Columbia, South Carolina 29208, USA*
[2]*Department of Chemical & Biomolecular Engineering, University of Connecticut, Storrs, Connecticut 06269, USA*
[3]*Instituto di Chimica dei Composti Organometallici (CNR-ICCOM), 50019 Sesto Fiorentino, Florence, Italy*
[4]*Department of Chemistry, University of Surrey, Guildford, GU2 7XH, United Kingdom*
[5]*The Wolfson Department of Chemical Engineering, Technion - Israel Institute of Technology, Haifa 3200003, Israel*

This work reports a high power, stable, completely Pt-free anion exchange membrane fuel cell (AEMFC) comprised of highly active catalysts – Pd-CeO_2/C at the anode and PdCu/C alloy at the cathode for the hydrogen oxidation and oxygen reduction reactions, respectively. The resulting AEMFC shows outstanding performance, reaching a peak power density of 1 W cm^{-2}, twice the value of the best performance for Pt-free cells reported in the literature to date. The AEMFC also shows a low voltage degradation rate when operated continuously for more than 100 h at a constant 0.5 A cm^{-2}, with a voltage degradation rate of only 2.5 mV h^{-1}, which is excellent when compared to nearly all of the AEMFCs reported in the literature to date. This combination of high performance and high stability in the absence of Pt-based catalysts represents a significant landmark in the progress of the AEMFC technology.
 [DOI: 10.1149/2.0071815jes]

Manuscript submitted June 13, 2018; revised manuscript received August 1, 2018. Published September 5, 2018. *This paper is part of the JES Focus Issue on Electrocatalysis — In Honor of Radoslav Adzic.*

Anion exchange membrane fuel cells (AEMFCs) have seen a rapid increase in interest in recent years as a possible low-cost energy conversion device.[1] Much of the interest in this technology comes from the expectation that AEMFCs can overcome the existing cost barriers[2,3] inherent to low temperature acidic polymer electrolyte membrane fuel cells. One step in doing this is to eliminate platinum from the electrodes either through the use of a historically less expensive precious metal such as palladium (see the supporting information and Figure S1 for more discussion and detail), or by using more naturally abundant platinum group metal (PGM)-free catalysts.[3–8] However, when transitioning away from Pt, it is very important not to markedly sacrifice catalyst activity or AEMFC performance.

High-performance AEMFCs have been recently reported, showing peak power values of ca. 1.4 W cm^{-2};[9,10] however, all of these state-of-the-art AEMFCs exclusively rely on Pt-based catalysts with Pt/C being the most common cathode catalyst and PtRu/C being the most common anode catalyst.[11–13] Unfortunately, very few studies reporting AEMFC performance with zero platinum loading can be found,[13] and the highest performing Pt-free AEMFCs showed a much lower performance, with peak power densities of 0.4–0.5 W cm^{-2}.[13–15]

In this work, new electrodes are developed, containing highly active Pd-based cathode and anode catalysts, and are combined with a radiation grafted anion exchange ionomer and membrane[10,16,17] to realize high performance AEMFCs that are completely Pt free. In fact, in this manuscript, a step change in performance is demonstrated over all other Pt-free AEMFCs reported to date. Achieving such high performance in these cells was not a straightforward application of many of our previous findings.[9,18,19] Using these new catalysts – particularly the application of Pd-CeO_2/C at the anode – required new learnings with regard to cell operation that are likely a function of different wettability of the CeO_2-containing support as well as the low Pd loading in the Pd-CeO_2/C catalyst (only 10%). Specific insights include the degree to which ionic resistance in the catalyst layers limits cell performance, the impact of temperature on the mass transport and kinetics of Pt-free AEMFCs and the response of these Pd-based cells to the application of backpressure (which is exactly opposite of Pt-based cells) – none of which have been reported previously.

Experimental

Synthesis of PdCu/C.—$Cu(acac)_2$ and $Pd(OAc)_2$ were used as the metal precursors. Benzyl alcohol was used as the solvent. Polyvinylpyrrolidone (PVP) and aniline were used as the capping reagent and reducing reagent, respectively. In a typical synthesis, 400 mg of PVP was added into 25 mL of benzyl alcohol. The mixture was rigorously sonicated until all of the PVP dissolved, after which 35 mg of Vulcan XC-72R was added to the liquid mixture, followed by a 10 min sonication until the formation of a homogenous suspension. 70 mg of $Cu(acac)_2$, 60 mg of Pd acetate (a 1:1 molar ratio of Cu:Pd) and 0.8 mL aniline were added into the suspension, followed by intense sonication until a homogenous dark blue solution was formed. The resulting solution was transferred to a 50 mL Teflon-lined autoclave. After a 24 h heating at 170°C, the autoclave was cooled down to room temperature with cold tap water. The resulting PdCu/C was washed with an ethanol-acetone (1:1 by volume) mixture three times, separated via centrifugation at 8000 RPM, and dried at 60°C under vacuum overnight. The PdCu/C particles were then thermally annealed at 200°C in a tube furnace in a pure H_2 atmosphere (H_2 flowrate = 40 cm^3 min^{-1}) for 5 h. A typical synthesis yielded approximately 70 mg of PdCu/C with a Pd:Cu molar ratio of 1:1, and a 40 wt% metal loading on carbon.

Synthesis of C-CeO_2 (50:50).—Vulcan XC-72 (4.0 g) was added to a solution of $Ce(NO_3)_3 \cdot 6H_2O$ (5.31 g) in 18.2 MΩ deionized H_2O (250 mL). The mixture was kept under stirring for 30 min and sonicated for 30 min. After adjusting the pH to 12 with 2 M aqueous KOH, the resulting suspension was stirred vigorously for 2 h. The solid product was separated by filtration and washed with H_2O until neutral pH was reached. The product was dried at 65°C and subsequently heated under air in a tube furnace at 250°C for 2 h. Cooling to room temperature was undertaken under a flow of Ar. The yield of CeO_2-C was 7.45 g.

Synthesis of Pd-CeO_2/C (10 wt% Pd).—CeO_2-C (4.0 g) was suspended in water (500 mL), stirred vigorously for 30 min and sonicated for 10 min. To this mixture, a solution of K_2PdCl_4 (1.38 g, 4.23 mmol)

=These authors contributed equally to this work.
*Electrochemical Society Student Member.
**Electrochemical Society Member.
zE-mail: dario@technion.ac.il; mustainw@mailbox.sc.edu

in H_2O (60 mL) was slowly added (1 mL min^{-1}) under vigorous stirring, followed by an addition of an aqueous solution of 2.5 M KOH (8.4 mL). Ethanol (50 mL) was then added to the resulting mixture, which was then heated at 80°C for 60 min. The desired product Pd-CeO_2/C was recovered by filtration, washed several times with deionized H_2O to neutrality and finally dried under vacuum at 40°C until a constant weight was achieved (Yield: 4.45 g).

Electrochemical measurements.—The electrochemical response of the synthesized catalysts was probed using thin film electrodes deposited onto a rotating disk electrode (RDE) in a custom three-electrode glass cell (Adams & Chittenden Scientific Glass) using a platinum mesh as the counter electrode and a double junction Ag/AgCl reference electrode (Pine Research Instrumentation). In the case of PdCu/C, the working electrode was prepared on a glassy carbon disk electrode with Pd loading of 12 μg cm^{-2} and a Nafion dispersion was used as a binder. For the Pt/C catalyst experiments, Pt/TKK (50 wt%, BASF) was used with a Pt loading of 19 μg cm^{-2}. Cyclic voltammograms (CVs) were collected at scan rate of 20 mV s^{-1} in N_2 purged aqueous 0.1 M KOH. ORR polarization curves were collected in O_2-purged aqueous 0.1 M KOH at scan rate of 10 mV s^{-1} with a rotation rate of 1600 RPM. In the case of Pd-CeO_2/C, linear sweep voltammetry experiments were performed in a Pyrex™ (Princeton Applied Research) glass cell filled with aqueous 0.1 M KOH solution into which N_2 or H_2 was bubbled (30 mL min^{-1}) for 30 min prior to each experiment. Ag/AgCl and Pt foil were applied as reference and counter electrode, respectively. All electrochemical studies were carried out using a Princeton 2273A potentiostat/galvanostat (Princeton Applied Research).

Membrane and gas diffusion electrode (GDE) fabrication.—The chloride-form ETFE-BTMA radiation grafted anion exchange membrane (AEM) synthesis was previously described in detail[10] and is summarized herein. The AEM was synthesized from a 25 μm thick ethylenetetrafluoroethylene (ETFE) sheet, which was first peroxidated in air using a total electron beam absorbed dose of 30 kGy, then immersed in a vinylbenzyl chloride (VBC, mixed *meta-*/*para*-isomer) solution to graft the VBC to the polymer backbone, and finally quaternized with a trimethylamine (TMA) solution. The chloride-form ETFE-BTMA anion exchange ionomer (AEI, ion-exchange capacity = 1.26 ± 0.06 meq g^{-1}) used was an (ETFE) powder with a particle size of 20–30 μm (peroixidated using an electron-beam absorbed dose of 70 kGy), radiation grafted with VBC and quaternized with TMA, a procedure previously reported in detail.[16] The gas diffusion layer (GDL) employed was Toray-060 with 5 wt% PTFE wetproofing.

To prepare the catalyst ink, first the AEI powder was ground for 10 min with a mortar and pestle, after which 100 mg–150 mg of PdCu/C supported catalyst or 250 mg of Pd-CeO_2/C supported catalyst was added to the AEI (ionomer loading of 20 wt% AEI) with 1 mL DI water (ultra-pure deionized H_2O with a resistivity of 18.2 MΩ cm). The resulting AEI-catalyst mixture was then ground in the mortar and pestle for 10 min, ensuring a texturally homogenous slurry. After this grind, 2 mL of 2-propanol (Fisher Chemical Optima) was added to the slurry, and the mixture was ground for 5 mins. To complete the ink, the slurry was combined with another 7 mL of 2-propanol in a LDPE vial, and homogenized in an ice-chilled ultrasonic bath (Fisher Scientific FS30H) for 1 h. GDEs were created through spray deposition of the catalyst ink on a larger area GDL, from which 5 cm^2 electrodes were cut. A final PGM loading of the electrodes was 0.4 mg cm^{-2} at the anode, and 0.6 mg cm^{-2} at the cathode, giving a total PGM loading of 1.0 mg cm^{-2}, which is lower than our previously-reported Pt based cells – 1.3 mg_{PGM} cm^{-2}. A more detailed GDE fabrication procedure has been previously reported.[9]

Anion exchange membrane fuel cell (AEMFC) assembly and testing.—Prior to assembly, the GDEs and AEMs were immersed in aqueous 1 M KOH electrolyte for 1 h, changing the solution every 20 min to ensure ion exchange of the membrane and ionomer (minimize residual Cl^- content). Excess aqueous KOH was removed with a laboratory cloth and the cells were assembled in Scribner fuel cell hardware (5 cm^2 active area, single serpentine flow pattern), and torqued to 5.1 N m with no prior hot pressing. 6-mil (150 μm) PTFE gaskets were used to achieve a 20% pinch on the membrane electrode assembly. Humidified H_2 and O_2 streams were supplied to the cell from an 850e Scribner Fuel Cell Test Station at a flow rate of 1.0 L min^{-1} for all tests. The cell temperature was tested at both 60°C and 70°C and the cell was operated at both atmospheric pressure (1.0 bar_a) and with a back pressure of 2.0 bar_g and 1.0 bar_g at the anode and cathode respectively. The heated follow lines between the fuel cell and test stand were maintained 5°C above the respective gas dew point. All of the i-V and i-P curves were collected under potentiostatic control with a scan rate of 10 mV s^{-1}. Linear sweeps – in lieu of point-by-point collection was used in order to better tease out flooding issues under water starved and flooded conditions. When the water management issues are well controlled, there is no significant difference between point by point and linear sweep polarization curves, which is shown in previous work for multiple high performing cells.[9] Additionally, tests were repeated after multiple hours and varying the testing conditions to ensure stability, recoverability, and repeatability.

Quantitative analysis of AEMFC polarization curves.—In investigating the polarization of these Pt-free AEMFCs, it is important to understand the fundamental contributions to cell behavior: kinetics, ohmic resistance and mass transport. Though researchers have deconvoluted the polarization curves into these constituents many different ways, many of which have be presented in the literature, one of the most straightforward methodologies to apply was published by Gasteiger et al.[20] in 2004. Their approach was adapted for use in this work, which is briefly described below.

First it is assumed that the polarization of an operating fuel cell is only a result of kinetic, ohmic, and mass transfer phenomena, in which case the operating cell voltage at any current can be represented by:

$$E_{cell} = E_{rev} - \eta_\Omega - \eta_k - \eta_{MT} \quad [1]$$

where E_{cell} is the operating cell voltage, E_{rev} is the thermodynamic reversible cell potential (1.20 V under the conditions used for the AEMFCs in this manuscript), and η_Ω, η_k, and η_{MT} represent the ohmic, kinetic, and mass transfer overpotentials, respectively. To extract each of the overpotentials represented in Equation 1, first the ohmic overpotential is isolated, which can be directly calculated at each point on the curve from the product of the high frequency resistance (R_{HFR}) – which is measured by a frequency response analyzer built into the Scribner fuel cell test stands – and the operating current (i), as shown in Equation 2:

$$\eta_\Omega = i R_{HFR} \quad [2]$$

The kinetic overpotential is extracted next, which can be isolated from the mass transfer overpotential at cell voltages greater than 0.85 V and operating currents less than 100 mA cm^{-2}, utilizing the assumption that mass transfer limitations are negligible in that region.[20] Under these conditions, Equation 1 can be simplified and the resulting data fit by the Tafel equation as shown in Equation 3:

$$E_{rev} - E_{cell} - \eta_\Omega = \eta_k \propto a + b \log i \quad [3]$$

where b is the Tafel slope. The final step of the deconvolution is to calculate the mass transfer overpotential, which is done by simply subtracting the kinetic and ohmic overpotentials from the reversible cell potential at all current densities:

$$\eta_{MT} = E_{rev} - \eta_\Omega - \eta_k \quad [4]$$

It should be noted that in this method the cell polarization due to hydroxide transport resistance within the catalyst layer, a component typically considered part of the ohmic resistance, is included in the mass transfer overpotential. Accounting for this ionic transfer resistance requires an AC impedance frequency sweep to measure, a technique that is not practical during a dynamic polarization experiment. In this deconvolution method, the catalyst layer ohmic transfer

resistance presents itself in the mass transport overpotential plot as the initial slope before the mass transport limiting current is reached.

Results and Discussion

Pd catalyst characterization and electrochemical testing.—The cathode catalyst utilized in this work is a Pd-Cu nanoparticle alloy supported on Vulcan XC-72R carbon black (PdCu/C) and the anode catalyst is comprised of metallic palladium nanoparticles supported on a ceria-carbon composite (Pd-CeO_2/C). The XRD patterns for the PdCu/C, Pd-CeO_2/C, and Pd/C as reference are shown in Figure 1A. The PdCu/C nanoparticles were primarily a 1:2 Pd:Cu B2-type ordered body-centered cubic. The XRD pattern for the Pd-CeO_2/C catalyst confirms the presence of crystalline Pd nanoparticles and ceria support. TEM images of the PdCu/C catalyst (Figure 1B) show that the PdCu particles were well dispersed on the Vulcan surface with an average particle diameter between 7–8 nm. TEM images of the Pd-CeO_2/C catalyst (Figure 1C) show that the CeO_2 particles were generally supported on the Vulcan surface and the Pd nanoparticles were accumulated preferentially on the CeO_2 portions leaving the carbon with very few Pd nanoparticles (particles size around 2.0 nm).

To investigate the electrochemical behavior of the PdCu/C catalyst, first, cyclic voltammograms (CVs) were recorded at room temperature in N_2-saturated 0.1 M KOH electrolyte at a sweep rate of 20 mV s^{-1} (Figure 2A). All potentials reported and discussed in this work are relative to reversible hydrogen electrode (RHE). The CV exhibited the two features that are characteristic of Pd: the first was related to hydrogen underpotential deposition (H_{upd}) between 0.05 V < E < 0.35 V and the second was Pd oxidation/reduction between 0.6 V < E < 0.9 V. Next, oxygen reduction reaction (ORR) polarization curves were collected from PdCu/C thin films supported on a glassy carbon RDE. The results are shown and compared to conventional Pt/C in Figure 2C. Compared to Pt/C, the PdCu/C catalyst exhibited a half-wave potential that was 50 mV more positive, indicating improved ORR kinetics[21] that can be ascribed to the synergistic effect of alloying Pd and Cu in the B2-type structure, where the lower resulting oxygen binding energy makes the dissociation of intermediate OOH species more facile.[22,23]

CVs for the Pd-CeO_2/C catalyst were also recorded at room temperature in N_2-saturated 0.1 M KOH electrolyte at a sweep rate of 20 mV s^{-1} (Figure 2B). It was observed that the H_{upd} potential shifted negatively by ca. 90 mV for the Pd-CeO_2/C catalyst relative to Pd/C, which suggested significant metal-support interactions where the surface H was bound less strongly when Pd was in the presence of CeO_2-C. The shift due to this metal-support interaction was even more significant than what was observed through alloying in Figure 2A. Weakening of the Pd-H binding energy promotes the hydrogen oxidation reaction (HOR) in alkaline media,[12,24] which led to much improved HOR kinetics, evidenced by the 150 mV s^{-1} improvement in half-wave potential in the RDE environment (Figure 2D). One likely explanation for this enhancement is that the presence of OH_{ad} species may help in promoting the hydrogen oxidation, which was pointed out in previous studies.[13–15]

Anion exchange membrane fuel cell testing with Pd-based electrodes.—Membrane electrode assemblies (MEAs) were prepared using solid powder anion conducting ionomers[16] and membrane[10] based on ethylenetetrafluoroethylene (ETFE) polymer backbone and a benzyltrimethyl ammonium (BTMA) headgroup. Two dispersions were made with Pd-CeO_2/C (10 wt% Pd) and PdCu/C (40 wt% PdCu) catalysts through successive grinding steps with the ionomer and addition of a mixture of deionized water and 2-propanol. The inks were then sprayed onto Toray 60 gas diffusion layers to form the electrodes (anode = Pd-CeO_2/C; cathode = PdCu/C), which were placed on opposite sides of the ETFE-BTMA anion exchange membrane and loaded into fuel cell hardware with a 5 cm^2 active area. It should be noted that the low fraction of Pd catalyst in the anode electrode can have a significant effect on the behavior of the cell and the triple phase boundary, as the active sites are more dispersed through the catalyst layer.

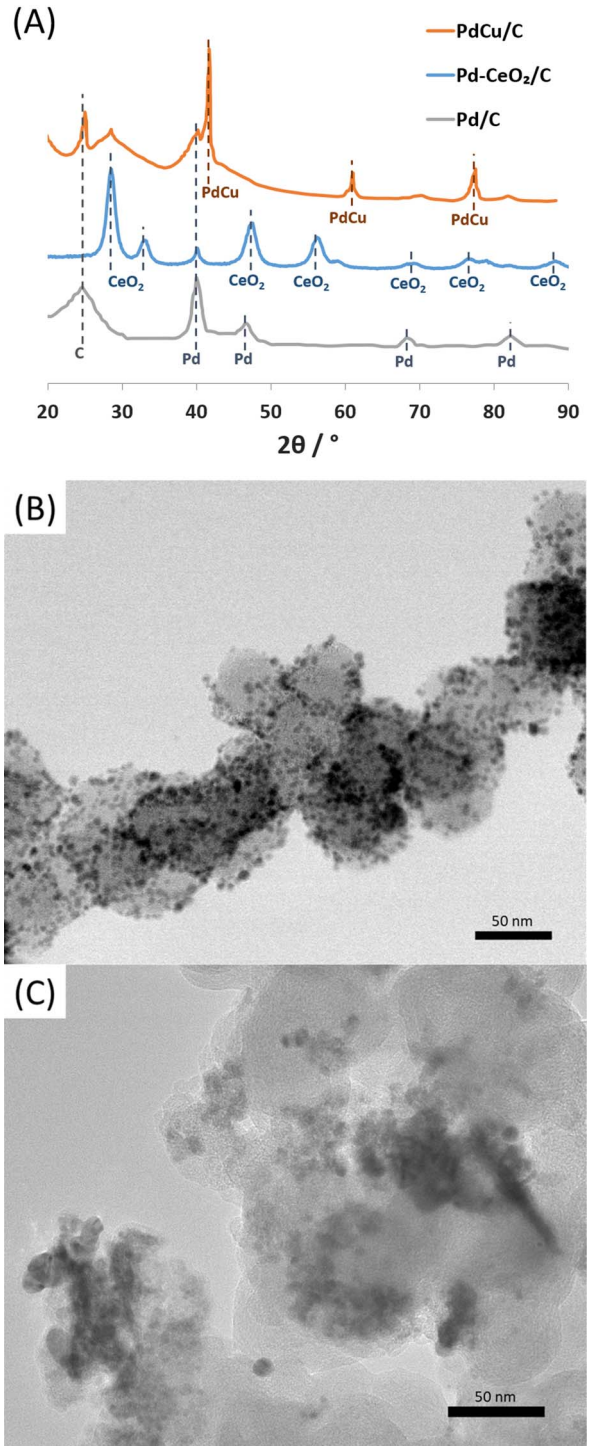

Figure 1. A) XRD patterns of PdCu/C and Pd-CeO_2/C showing a mixed phase (lab-synthesized Pd/C is also shown as reference); TEM images showing the morphology of B) PdCu/C and C) Pd-CeO_2/C.

After the AEMFCs were assembled, they were initially brought to 60°C with a Scribner 850e fuel cell test station, humidified, equilibrated, and optimized to anode/cathode dewpoints of 49°C/50°C. Immediately after optimization (Figure S5 in the Supporting Information), the cell was polarized without back pressure (labeled as "60C-nBP" in Figures 3A–3B), and a peak power density of 500 mW cm^{-2} was achieved. The polarization curves were deconvoluted into

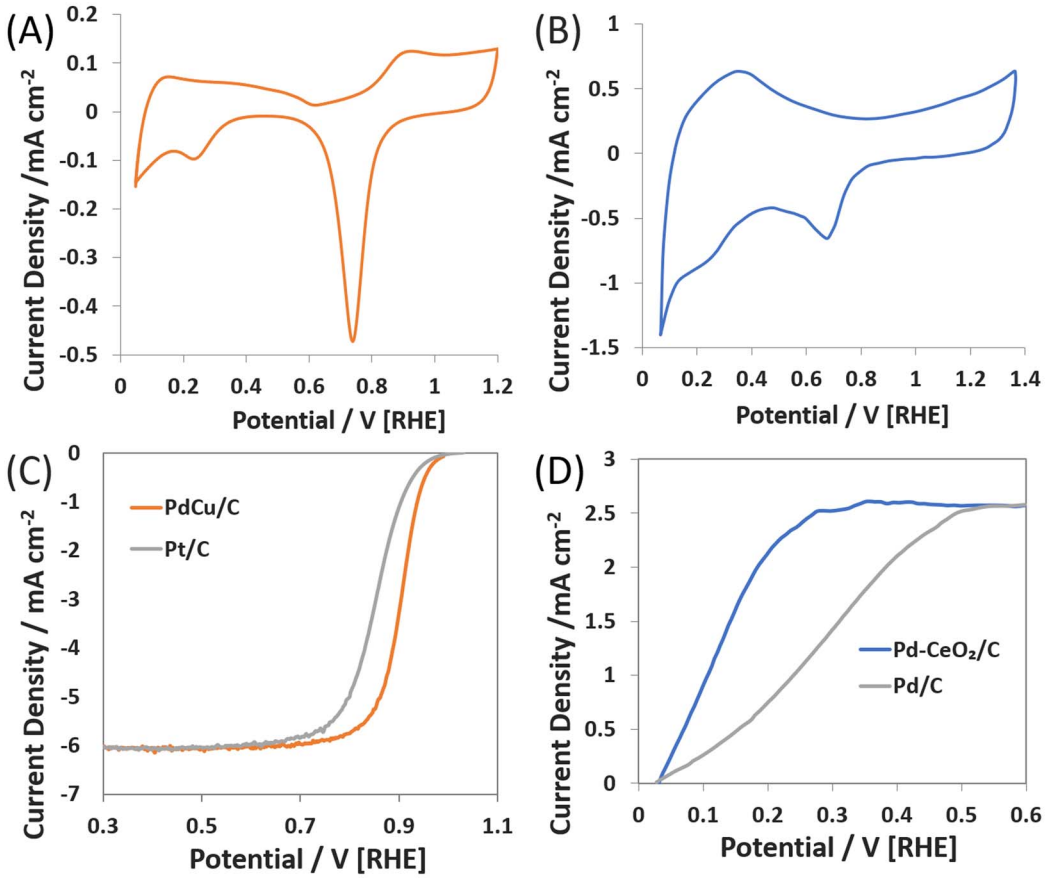

Figure 2. Cyclic voltammogram of A) Pd-Cu/C and B) Pd-CeO_2/C in N_2-saturated 0.1 M KOH solution at room temperature; C) ORR polarization curves of PdCu/C and Pt/C in O_2-saturated 0.1 M KOH at 1 mV s^{-1}, 1600 rpm; D) HOR polarization curves of Pd-CeO_2/C and Pd/C in H_2-saturated 0.1 M KOH at 10 mV s^{-1}, 1600 rpm. For all scans the ionomer loading was 20 wt% and the Pd and Pt loadings were 12 μg cm^{-2} and 19 μg cm^{-2} respectively.

their mass transfer (MT), ohmic, and kinetic overpotentials (Figures 3C–3E) and it was discovered that the MT overpotential for this electrode was significantly higher than electrodes prepared with Pt-based catalysts using the same ionomer[18] – particularly at lower currents (<1 A cm^{-2}). Because of the method used to deconvolute the overpotentials, the low current region of the mass transport plot is dominated by the hydroxide transfer resistance in the catalyst layers. High ionic resistance in the catalyst layer is often indicative of catalyst layer dryout, which was likely caused by convective dryout at the low optimum cell dew points, and perhaps consumption at the cathode as well.

One approach to decreasing the rate of convective water loss from the catalyst layers is to apply backpressure the cell, since it allows for an increase in the absolute amount of water present in cell while maintaining the relative balance of the reacting gases. Therefore, backpressure was applied to the cell – and the cell was again polarized. The backpressure conditions that yielded the highest performance were 3.0 bar_a at the anode and 2.0 bar_a at the cathode; backpressure optimization and its effects are thoroughly shown in Figure S6 in the Supporting Information. It can be seen in Figure 3 that the AEMFC with optimized backpressurization (denoted as "60C-BP") has significantly improved the hydroxide transfer resistance as well as decreased the kinetic overpotential through an increase in the partial pressure of the H_2 and O_2. These reductions in overpotentials led to a 50% increase in the peak power density to 750 mW cm^{-2}, however, one negative side effect of applying backpressure and increasing the total amount of water in the electrode was that the ability of the electrodes to reject the liquid water that was produced from the anode reaction at high currents was diminished. Hence, the slope of the bulk mass transport loss at higher current was much more steep (Figure 3C).

The success of adding back pressure, especially at the high value of 3.0 bar_a at the anode, runs counter to what has been observed with Pt-based electrodes using the same ionomer and membrane.[9,10,12,18,25,26] This suggests that the catalyst dispersion and loading can play a significant role in dictating the response of AEMFC anodes to the water that is generated since the application of back pressure will enhance the total amount of water in the catalyst layers, which may also allow for reacting gases with even lower dew points to be fed to the cell – both new learnings for AEMFCs.

Although the performance above on its own would be the highest reported for Pt-free AEMFCs to date,[13] the shape of the polarization curve in combination with the steep increase in the mass transport resistance (Figure 3C) at moderate current density (~1.5 A cm^{-2}) suggests that some degree of water flooding is occurring in the electrodes. At these current densities, the cell is producing a significant amount of water at the anode, which is used to both provide the reacting cathode water (via back-diffusion) as well as maintain membrane humidification.[18] Hence, it is not necessary to provide as much water to the cell through the reacting gas feeds and improved performance can be expected by reducing the amount of water supplied to the anode.[9,18]

Therefore, the dew points of the reacting gases were systematically reduced (Figure S7 in the Supporting Information) until the optimal cell performance was achieved at anode/cathode dew points of 39°C and 41°C (relative humidity (RH) = 35% and 39%), respectively. The resulting polarization and power curves are labeled as "60C-BPo" in Figures 3A–3B. The result of optimizing the anode/cathode dew points was that the limiting current density was increased by 33% (1.8 A cm^{-2} to 2.4 A cm^{-2}) and the peak power density was increased by 10% (to 0.83 W cm^{-2}).

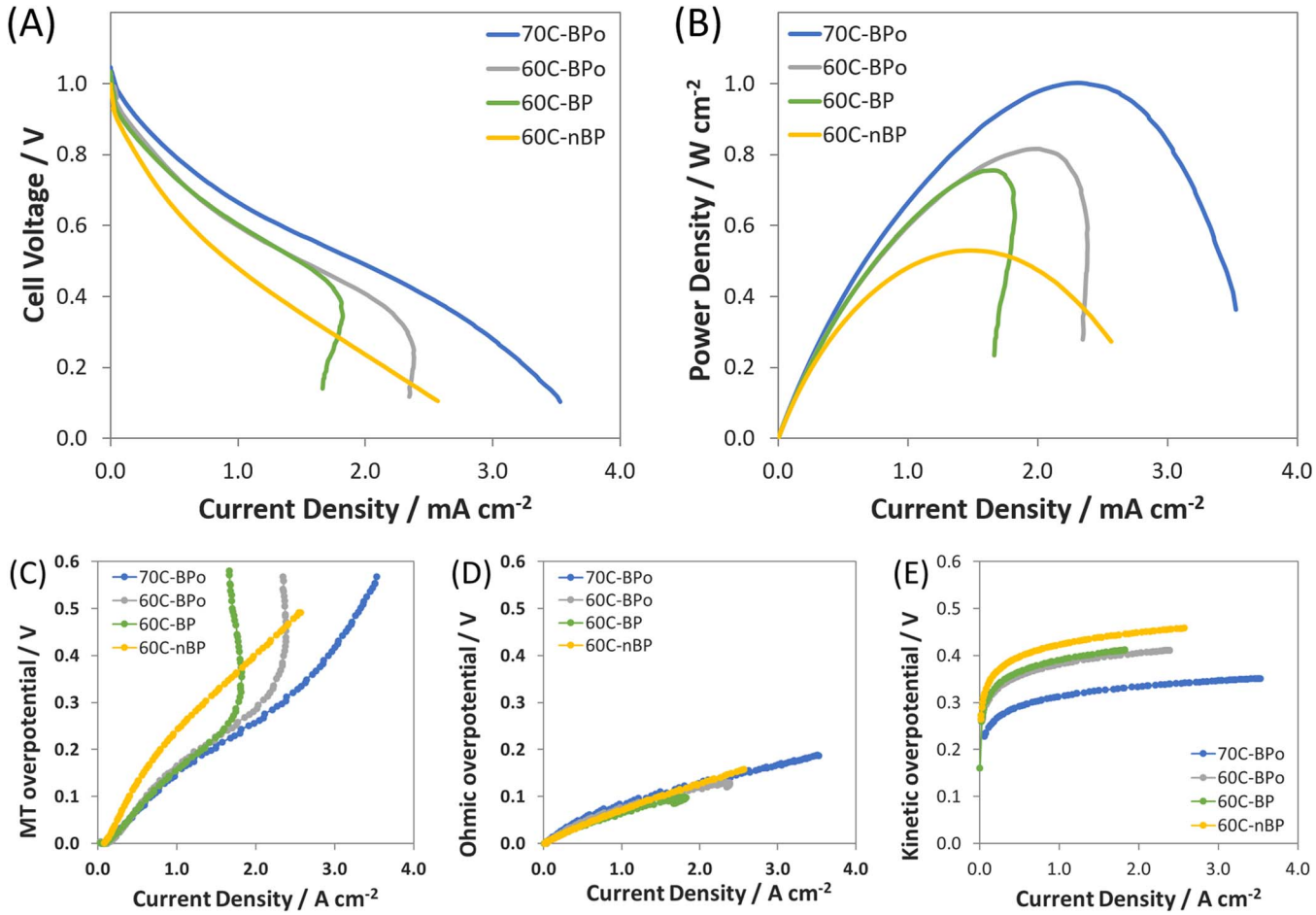

Figure 3. A) i-V and B) i-Power curves (10 mV s^{-1} forward scans from open circuit voltage to 0.1 V) of Pt-free AEMFCs assembled with a radiation grafted ETFE-BTMA membrane, a 10% Pd-CeO_2/C anode (0.42 mg cm^{-2} Pd-loading), and a 40% PdCu/C cathode (0.58 mg cm^{-2} Pd-loading), and both electrodes contained 20 wt% ETFE-BTMA ionomer. H_2 and O_2 were fed at 1.0 L min^{-1} to the anode and cathode respectively. The cells were run at atmospheric pressure or with 3.0 bar_a at the anode and 2.0 bar_a at the cathode, indicated in the plot as "-nBP" for no backpressure and "-BP" or "-BPo" for cells with backpressure applied. The cell temperature and anode/cathode dewpoints were: 60°C and 49°C/50°C (60C-nBP and 60C-BP); 60°C and 39°C/41°C (60C-BPo); and 70°C and 40°C/42°C (70C-BPo); The polarization curves were deconvoluted into their C) mass transfer (MT), D) ohmic, and E) kinetic overpotentials, demonstrating the effect of the temperature on cell behavior.

The polarization and power curves in Figures 3A–3B were further analyzed by deconvoluting them to extract the mass transport, ohmic and kinetic overpotentials (Figures 3C–3E). Two things were immediately clear. First, manipulating the reacting gas dew points has a negligible effect on the electrode kinetics. Second, under these conditions, the kinetic resistance mostly controls cell behavior, though the mass transport resistance is also significant. In fact, these all-Pd AEMFCs did show slightly higher kinetic overpotentials than Pt-based catalysts at the same temperature over the entire polarization range.[18]

Since it can be expected that both the electrode kinetics and the mass transfer resistance would be improved by increasing the cell temperature, the AEMFC operating temperature was increased to 70°C. The dew points were again optimized (Figure S8 in the Supporting Information), and the AEMFC achieved a peak power density of 1.0 W cm^{-2} (at 0.42 V) and a mass-transport limited current density of 3.5 A cm^{-2} – both new records in the literature for Pt-free AEMFCs. The polarization and power curves are labeled as "70C-BPo" in Figures 3A–3B. From a catalysis perspective, the increase in cell temperature led to significantly lower kinetic overpotentials (Figure 3E) over the entire data set. Additionally, the high temperature operation combined with the low relative humidity reacting gases allowed for electrode flooding to be relaxed and resulted in a decrease in the mass transfer overpotential as well (Figure 3C). Another interesting point is that the AEMFC performed so well that the water produced at the anode was nearly completely sufficient to internally humidify the cell – leading to optimum dew points for the anode/cathode of 40°C/42°C (RH = 26%/29%), astonishingly low and the lowest reported relative humidities for an operating AEMFC to date.

The AEMFCs with the Pd-based anode and cathode catalysts were also tested for longevity at a constant 0.5 A cm^{-2} current density for 100 h (Figure 4). Promisingly, during this time the cell was able to retain more than 75% of its initial operating voltage, even though the chosen current density of this test was the highest applied for any AEMFC longevity test to date,[13] therefore representing a very harsh condition for long-term operation. The small decrease of voltage during cell testing can be explained by an increase in the high frequency resistance of the cell (HFR, Figure 4), a measure of the membrane contribution to the cell overpotential. This increase in HFR is explained by either a slow loss of membrane water and/or membrane/ionomer degradation.[27,28]

Conclusions

In summary, this study is the first in the literature to demonstrate completely Pt-free AEMFCs that show excellent stability as well as very high performance ~1 W cm^{-2} – comparable to the state-of-the-art Pt cells. The peak power density achieved in this work was twice that of the best Pt-free cells in the literature to date. The cell was also

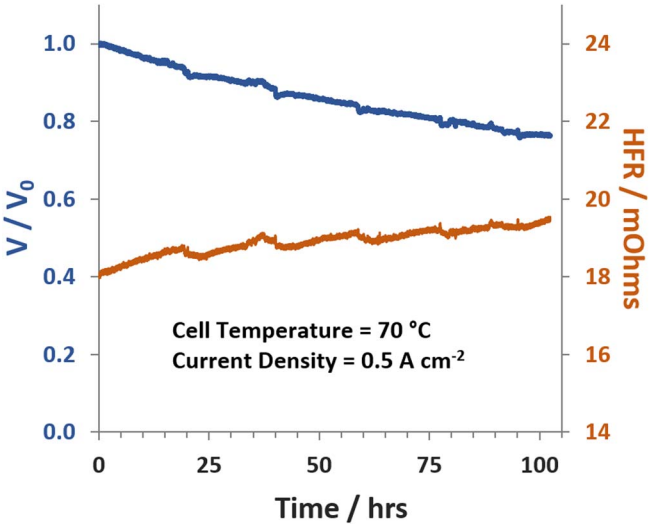

Figure 4. Stability test for the Pt-free AEMFC with Pd-CeO2/C and PdCu/C catalysts, and ETFE-BTMA membrane. Voltage was normalized by its initial voltage at time = 0 (V_o). Anode and cathode Pd loading: 0.4 mg cm^{-2}. H_2 and O_2 were flowed to the anode (3 bar_a) and cathode (2 bar_a) at 1.0 L min^{-1}. Cell temperature: 70°C; anode/cathode dew points: 62°C / 62°C.

able to achieve very good stability at a high temperature and current density. This high performing Pt-free cell represents a significant landmark in the development progress of AEMFC technology. We expect that in the very near future more and more studies will be focused on Pt-free AEMFCs, finally removing Pt as a prerequisite starting point to achieve high performing polymer fuel cells.

Acknowledgments

First and foremost, Prof. Mustain would like to send a personal note to Dr. Radoslav Adzic. It is an honor to be able to contribute this article to this JES focus issue in your name. You have been a great inspiration to me from early in my career when I was reading your papers a graduate student until today as you have been a valued friend, colleague and mentor. You are not only one of the most accomplished electrochemists in the world, but also a wonderful person. I wish you nothing but the best and sincerely thank you for everything you have done for me.

The authors gratefully acknowledge the financial support of the US DOE Early Career Program (Award Number DE-SC0010531) for the effort expended by T.J.O., X.P., and W.E.M. to synthesize the PdCu/C catalyst and to perform the fuel cell experiments. The ETFE-based materials used were developed and produced by the University Surrey team and this effort was funded by the UK's Engineering and Physical Sciences Research Council (EPSRC grant EP/M014371/1). This work was also partially funded by the Nancy & Stephan Grand Technion Energy Program (GTEP); by the European Union's Horizon 2020 research and innovation program [grant number 721065]; by the Ministry of Science, Technology & Space of Israel through the M.Era-NET Transnational Call 2015, NEXTGAME project [grant number 3-12940] and through grant number 3–12948; by the Israel Science Foundation (ISF) [grant number 1481/17]; by the 2nd Israel National Research Center for Electrochemical Propulsion (INREP2-ISF); and by the Ministry of National Infrastructure, Energy and Water resources of Israel [grant no. 3-13671]. We also thank the Ente Cassa di Risparmio di Firenze (project EnergyLab).

The authors would like to sincerely thank B.S. Pivovar and K.C. Neyerlin at the National Renewable Energy Laboratory for helpful and enlightening discussions. We would also like to note the T.J.O. and X.P. contributed equally to this work.

ORCID

Travis J. Omasta https://orcid.org/0000-0002-8002-6520
John R. Varcoe https://orcid.org/0000-0001-9898-0235
Dario R. Dekel https://orcid.org/0000-0002-8610-0808
William E. Mustain https://orcid.org/0000-0001-7804-6410

References

1. J. R. Varcoe, P. Atanassov, D. R. Dekel, A. M. Herring, M. A. Hickner, P. A. Kohl, A. R. Kucernak, W. E. Mustain, K. Nijmeijer, K. Scott, T. Xu, and L. Zhuang, *Energy Environ. Sci.*, **7**, 3135 (2014).
2. B. P. Setzler, Z. Zhuang, J. A. Wittkopf, and Y. Yan, *Nat. Nanotechnol.*, **11**, 1020 (2016).
3. S. Gottesfeld, D. R. Dekel, M. Page, C. Bae, Y. Yan, P. Zelenay, and Y. S. Kim, *J. Power Sources*, **375**, 170 (2018).
4. L. Wang, J. J. Brink, and J. R. Varcoe, *Chem. Commun.*, **53**, 11771 (2017).
5. S. A. Kabir, K. Lemire, K. Artyushkova, A. Roy, M. Odgaard, D. Schlueter, A. Oshchepkov, A. Bonnefont, E. Savinova, D. Sabarirajan, P. Mandal, E. Crumlin, I. V Zenyuk, P. Atanassov, and A. Serov, *J. Mater. Chem. A*, **5**, 24433 (2017).
6. Z. Zhuang, S. A. Giles, J. Zheng, G. R. Jenness, S. Caratzoulas, D. G. Vlachos, and Y. Yan, *Nat. Commun.*, **7**, 1 (2016).
7. R. Gokhale, Y. Chen, A. Serov, K. Artyushkova, and P. Atanassov, *Electrochem. Commun.*, **72**, 140 (2016).
8. P. Song, Y. Wang, J. Pan, W. Xu, and L. Zhuang, *J. Power Sources*, **300**, 279 (2015).
9. T. J. Omasta, L. Wang, X. Peng, C. A. Lewis, J. R. Varcoe, and W. E. Mustain, *J. Power Sources*, **375**, 205 (2018).
10. L. Q. Wang, E. Magliocca, E. L. Cunningham, W. E. Mustain, S. D. Poynton, R. Escudero-Cid, M. M. Nasef, J. Ponce-González, R. Bance-Souahli, R. C. T. Slade, D. K. Whelligan, and J. R. Varcoe, *Green Chem.*, **19**, 831 (2017).
11. E. S. Davydova, S. Mukerjee, F. Jaouen, and D. R. Dekel, *Submitt. to ACS Catal.* (2018).
12. Y. Wang, G. Wang, G. Li, B. Huang, J. Pan, Q. Liu, J. Han, L. Xiao, J. Lu, and L. Zhuang, *Energy Environ. Sci.*, **8**, 177 (2015).
13. D. R. Dekel, *J. Power Sources*, **375**, 158 (2018).
14. H. A. Miller, F. Vizza, M. Marelli, A. Zadick, L. Dubau, M. Chatenet, S. Geiger, S. Cherevko, H. Doan, R. K. Pavlicek, S. Mukerjee, and D. R. Dekel, *Nano Energy*, **33**, 293 (2017).
15. M. Alesker, M. Page, M. Shviro, Y. Paska, G. Gershinsky, D. R. Dekel, and D. Zitoun, *J. Power Sources*, **304**, 332 (2016).
16. S. D. Poynton, R. C. T. Slade, T. J. Omasta, W. E. Mustain, R. Escudero-Cid, P. Ocón, and J. R. Varcoe, *J. Mater. Chem. A*, **2**, 5124 (2014).
17. Y. Zheng, U. Ash, R. P. Pandey, A. G. Ozioko, J. Ponce-González, M. Handl, T. Weissbach, J. R. Varcoe, S. Holdcroft, M. W. Liberatore, R. Hiesgen, and D. R. Dekel, *Macromolecules*, acs.macromol.8b00034 (2018).
18. T. J. Omasta, A. M. Park, J. M. Lamanna, Y. Zhang, X. Peng, L. Wang, D. L. Jacobson, J. R. Varcoe, D. S. Hussey, B. S. Pivovar, and W. E. Mustain, *Energy Environ. Sci.*, **11**, 551 (2018).
19. T. J. Omasta and W. E. Mustain, *Water and ion transport in anion exchange membrane fuel cells*, (2018).
20. H. A. Gasteiger, J. E. Panels, and S. G. Yan, *J. Power Sources*, **127**, 162 (2004).
21. S. Guo, S. Zhang, and S. Sun, *Angew. Chemie - Int. Ed.*, **52**, 8526 (2013).
22. F. Fouda-Onana, S. Bah, and O. Savadogo, *J. Electroanal. Chem.*, **636**, 1 (2009).
23. J. Wu, S. Shan, J. Luo, P. Joseph, V. Petkov, and C. J. Zhong, *ACS Appl. Mater. Interfaces*, **7**, 25906 (2015).
24. J. Durst, A. Siebel, C. Simon, F. Hasché, J. Herranz, and H. A. Gasteiger, *Energy Environ. Sci.*, **7**, 2255 (2014).
25. L. Wang, J. J. Brink, Y. Liu, A. M. Herring, J. Ponce-González, D. K. Whelligan, and J. R. Varcoe, *Energy Environ. Sci.*, 2154 (2017).
26. A. M. Park, Z. R. Owczarczyk, L. E. Garner, A. C. Yang-Neyerlin, H. Long, C. M. Antunes, M. R. Sturgeon, M. J. Lindell, S. J. Hamrock, M. Yandrasits, and B. S. Pivovar, *ECS Trans.*, **80**, 957 (2017).
27. D. R. Dekel, M. Amar, S. Willdorf, M. Kosa, S. Dhara, and C. E. Diesendruck, *Chem. Mater.*, **29**, 4425 (2017).
28. D. R. Dekel, S. Willdorf, U. Ash, M. Amar, S. Pusara, S. Dhara, S. Srebnik, and C. E. Diesendruck, *J. Power Sources*, **375**, 351 (2018).